BIBECHANA
ISSN 2091-0762 (Print), 2382-5340 (Online)
Journal homepage: http://nepjol.info/index.php/BIBECHANA
Publisher: Department of Physics, Mahendra Morang A.M. Campus, TU, Biratnagar, Nepal

Phonon dynamics of $Zr_{67}Ni_{33}$ and $Fe_{80}B_{20}$ binary glassy alloys

Aditya M. Vora[1*], Alkesh L. Gandhi[2]**
[1]Department of Physics, University School of Sciences, Gujarat University, Ahmedabad, 380 009, Gujarat, India.
[2]Department of Physics, B. V. Shah (Vadi Vihar) Science College, C. U. Shah University, Wadhwan, 363 002, Gujarat, India.
[*]Email: amvora@gujaratuniversity.ac.in, voraam@gmail.com
[**]Email: gandhi.alkesh.jain@gmail.com

Article Information:
Received: May 4, 2020
Accepted: June 17, 2020

Keywords:
Bulk metallic glass
Model potential
Interatomic pair potential
Phonon dispersion curve (PDC)
Thermodynamic properties

ABSTRACT
Binary amorphous alloys are the primary bulk metallic glasses (BMGs). Two binary BMGs $Zr_{67}Ni_{33}$ and $Fe_{80}B_{20}$ have been studied in the present work using the pseudo- alloy-atom (PAA) model based on the pseudopotential theory. Some important thermodynamic properties like Debye temperature and elastic properties like elasticity moduli and Poisson's ratio at room temperature are theoretically computed with the help of pseudopotential theory from the elastic limit of the phonon dispersion curves (PDCs). The collective dynamics of longitudinal and transverse phonon modes are investigated in terms of eigenfrequencies of the localized collective modes. The presently computed results are compared with the other such data including theoretically generated results from the molecular dynamics at different temperatures as available in the literature and an acceptable agreement is found.

DOI: https://doi.org/10.3126/bibechana.v18i1.28760

1. Introduction

Generally, the bulk metallic glasses (BMGs), which are non-crystalline metallic alloys, can be made-up with low cooling rates in many alloy systems. A metallic material is formed by the basic units of well-arranged metallic microstructures designed by the single-crystal grains of varying sizes. An alloy is produced by melting the constituent metal elements in predefined proportions followed by the solidification process. The solidification process of an amorphous alloy has a deep impact on its properties and structure at the corresponding temperature. So, the data of the physical properties of the molten alloys, before its solidification, is necessary for the development of a BMG with predefined characteristics. The properties of an alloy are fully dependent on the crystallization procedure and the final metallic microstructure, where both are determined by the selection of cooling pattern and the adopted thermal treatments. Unlike conventional crystalline alloys, a BMGs is

produced by quenching the alloy melt below its crystalline temperature by preventing the regular long-range arrangement with crystallization. The quickly frozen alloy-melt keeps the precursor liquid structure. Thus, the BMGs are said to be solids with liquid-like non-crystalline structure at the atomic or molecular level, which makes them highly resistant to permanent distortion and makes them more than twice tougher to its crystalline counterpart. In recent decades, the neutron scattering data from short-wavelength phonons in many BMG-configurations have been increasingly available. There are found an interesting similarity between the scattered neutron spectra of liquids and that of amorphous or crystalline solids near their melting point. Further, the theory of lattice dynamics is equally and successfully applied to the ordered crystalline as well as amorphous materials [1-32]

1.1 $Zr_{67}Ni_{33}$ BMG

In the binary transition metal-metal alloy systems i.e. Zr-Ni BMG is a unique one and its crystallization temperature is higher than the glass transition temperature (652K) under the heating conditions. Suck et al. [33] have studied longitudinal phonon dispersion mode of $Zr_{67}Ni_{33}$ glass by neutron inelastic scattering (NIS) method. While, Gupta et al. [13] have theoretically studied the phonon dispersion curves (PDCs) of such glass using Hubbard-Beeby (HB) [30] and Bhatia-Singh (BS) ([28] computational approaches and compared their outcomes with the results achieved through molecular dynamics (MD) simulation by Aihara et al. [15,16] . Also, they have found that there is a good agreement between the experimentally observed and theoretically computed data. Otomo et al. [17] have studied the dynamical structure factors and collective excitations of $Zr_{67}Ni_{33}$ glass with NIS method. Similarly, Lad and Pratap [18] have theoretically investigated the PDC of Zr-Ni BMG with model potential formalism using TG [31,32] and BS [28] approaches and got the results very close to the experimental and theoretical data available in the literature. While, Vora and co-workers [1-12] have evaluated the collective dynamics of some BMGs using Ashcroft's empty core model pseudopotential [34] Singh et al. [19] have examined Zr-Ni BMG with HB [30], TG [31,32] and BS [28] approaches using a newly constructed free model potential, which is, in fact, the alteration of the Ashcroft's model potential [34] only. The electronic structure, bonding and 3D atomic structure of $Zr_{67}Ni_{33}$ BMG were studied by Sugita et al. [20]. Very recently, Gandhi and Vora [6-10] have reported vibrational dynamics of some binary to hexanary BMGs using model pseudopotential theory. The interest in the Zr-based BMGs has been growing due to their superior mechanical properties like high fracture resistance, good corrosion resistance and micro-formability, which make them a favorable choice for various applications including high field superconducting magnets and the place where brittle alloys are not used [19,20].

1.2 $Fe_{80}B_{20}$ BMG

The metal-metalloid type $Fe_{80}B_{20}$ BMG, mainly referred to be as Metglas-2605, is produced by the rapid solidification process. It is a ferromagnetic with the good soft magnetic property having a high yield strength of ~3630 MPa, high elastic stiffness, and thermal stability, which all together make it superior to many other commercial binary BMGs. Though a little plasticity is its minor drawback, the low-cost $Fe_{80}B_{20}$ BMG is preferable for structural applications [21]. In the early 80's, Devis et al. [35] have experimentally studied properties of $Fe_{80}B_{20}$ BMG. Dimitrov et al. [22] and Agarwal et al. [23, 24] have carried out a limited study of this BMG. While, Vora [3] has theoretically studied $Fe_{80}B_{20}$ using all three theoretical approaches of PDCs.

Considering the multilevel applications of the BMGs, the vibrational dynamics of two binary BMGs $Zr_{67}Ni_{33}$ and $Fe_{80}B_{20}$ are reported in the current work. The well-behaved Shaw's optimized constant-core model pseudopotential [36] is employed using a self-consistent phonon scheme by relating multiple scattering and phonon eigenfrequencies. Such phonon frequencies

represent many-body correlation functions of atoms and concerned interatomic potential. To study the screening dependency on the aforesaid properties, the most effectively used five different local field correction (correlation) functions namely Hartree (H) [37], Taylor (T) [38] Ichimaru-Utsumi (IU) [39] and Sarkar *et al.* (S) [40] have been adopted to determine the effect of exchange and correlation on the bare ion potential. These screening functions help us to investigate the screening influence on the vibrational dynamics of the selected binary BMGs. Three independent computational approaches viz. Hubbard-Beeby (HB) [30], Takeno-Goda (TG) [31, 32], Bhatia-Singh (BS) [28] and Shukla and Campnha [29] have been employed to generate PDCs of said binary BMGs. The important thermodynamic and elastic properties viz. longitudinal sound velocity (υ_L), transverse sound velocity (υ_T), Young's modulus (Y), isothermal bulk modulus (B_T), rigidity modulus (K), Poisson's ratio (σ) and Debye temperature (θ_D) have been computed using the long wavelength limits of PDCs.

2. Computational methodology

The pseudopotential perturbation theory is an accepted tool for determining properties of amorphous alloys. As far as analytical calculations are concerned, many approximations based on model approaches are available to study the BMGs [1-11]. Shaw's optimized constant-core model pseudopotential [36] along with five different local field correction functions viz. H, T, IU, F and S have used for studying the screening influence on the said properties of the selected BMGs.

Here, the three theoretical approaches, namely HB [30], TG [31,32] and BS [28] have been extensively employed to study the phonon dispersion and collective excitations in binary BMGs. However, Hubbard and Beeby (HB) [30] have derived expressions for the longitudinal and transverse phonon eigenfrequencies by examining collective motion in the amorphous liquid system as a generalization of the phonon theory of solids using a random phase approximation. In which, the product of the static pair correlation function and the second order derivative of the interatomic potential is peaked near the hard-core radius. While, Takeno and Goda (TG) [31, 32] have expressed longitudinal and transverse phonon eigenfrequencies in terms of many-body correlation functions of atoms and interatomic potentials in amorphous solids. Bhatia and Singh (BS) [28, 29] have proposed a phenomenological model to determine the longitudinal and transverse phonon eigenfrequencies in amorphous solids.

In most of such studies, the pseudopotential parameters are evaluated in such a way that it can generate the comparable results of the pair correlation function (PCF) (g(r)) and PDCs, which are found to be in good agreement with experimental data. Mostly, Vegard's law is used to explain electron-ion interactions for binary BMGs. However, the well suitable pseudo-alloy-atom (PAA) model explains such interactions vary precisely. Hence, in the present article, the PAA model is used to investigate the phonon dynamics of A_xB_{100-x} binary BMG systems [1-11].

Considering these binary combinations of amorphous alloys to be mono-component fluids, the effective ion-ion interactions are given by [1-11],

$$V(r) = \frac{Z^2e^2}{r} + \frac{2}{\pi}\int F(q)\, e^{-iqr}\, dq \qquad (1)$$

where, $F(q)$ is the characteristics wave number, q is the space vector. The first and second terms in the above equation represent Coulombic interactions between ions and indirect interactions between conduction electrons, respectively. The pseudopotential perturbation along with the linear screening theory provides the basis of interatomic pair potential. The free-electron theory of metals has been extended to introduce the effects of amorphous structure. The presently computed interatomic pair potential (V(r)), based on the

extended theory of Wills-Harrison model [41] for $V(r)= V_s(r) + V_b(r) + V_r(r)$

$$V(r) = \left\{\frac{Z_s{}^2 e^2}{r} + \frac{\Omega_0}{\pi^2}\int F(q)\left[\frac{\sin(qr)}{(qr)}\right]q^2\,\mathrm{dq}\right\} + \left\{-Z_d\left[1-\frac{Z_d}{10}\right]\left(\frac{12}{N_c}\right)^{\frac{1}{2}}\left(\frac{28.6}{\pi}\right)\left(\frac{2\,r_d^3}{r^5}\right)\right\} + \left\{Z_d\left(\frac{450}{\pi^2}\right)^2\left(\frac{r_d^6}{r^8}\right)\right\} \quad (2)$$

where $V_s(r)$ is the s-electron contribution. The term $V_b(r)$ considers the Friedel-model band broadening contribution to the transition metal cohesion and $V_r(r)$ came from the repulsion of the d-electron muffin-tin orbital on different sites owing to their non-orthogonality. Also, the Z is the valence and Ω_0 the atomic volume of the BMGs, respectively. The self-consistent band structure calculation can provide the partials-density of states which can be used to obtain Z_s. The characteristics energy wave number term $F(q)$, with q as the q-space vector, under integration in the above equations, can be written as [1-11],

$$F(q) = \frac{-\Omega_0 q^2}{16\pi}\,|W_B(q)|^2\,\frac{[\varepsilon_H(q)-1]}{\{1+[\varepsilon_H(q)-1][1-f(q)]\}}, \quad (3)$$

where $W_B(q)$, $\varepsilon_H(q)$ and $f(q)$ are the bare ion potential, the Hartree dielectric response screening function [37] and the local field correction functions needed to introduce the exchange and correlation effects, respectively. Shaw's model potential used in the present work is of the form [36]

$$W_B(q) = -\frac{8\pi Z}{\Omega_0 q^2}\left[\frac{\sin qr_c}{qr_c}\right] \quad (4)$$

where, the potential parameter is computed by $r_c = (0.51)\,r_S\,\mathrm{Z}^{-1/3}$ [1-2].

Here, Wigner-Seitz radius of the BMG is given by

$$r_s = \left({}^{3\Omega_0}/_{4\pi Z}\right)^{1/3}$$

For BMGs, the PCF (g(r)) discloses much useful information about the inter-particle radial correlation, structure and further, that predicts the electrical, elastic, thermodynamic and other physical properties. Either it is obtained by using X-ray diffraction or by neutron scattering experimentally [25-27,42] theoretically [1-12, 23-24, 43] from interatomic pair potentials.

the BMGs is given by,

The vibrational dynamics of the aforementioned binary BMGs are studied by computing the longitudinal and transverse phonon eigenfrequencies, where the derivative of the interatomic pair potential (V(r)) in combination with PCF (g(r)) are used to compute the PDCs. The product of the static pair correlation function (g(r)) and the second order derivative (V''(r)) of the interatomic potential is peaked at the hard-sphere diameter. The rapid atomic motions of a disordered amorphous systems are very important because their structural, thermodynamic and transport properties are described by collective atomic motions.

According to HB [30]-approach, the expressions for the two components of the phonon frequencies i.e. longitudinal and transverse are computed from [30],

$$\omega_L^2(q) = \omega_E^2\left[1 - \frac{\sin(q\sigma)}{q\sigma} - 6\,\frac{\cos(q\sigma)}{(q\sigma)^2} + 6\,\frac{\sin(q\sigma)}{(q\sigma)^3}\right] \quad (5)$$

$$\omega_T^2(q) = \omega_E^2\left[1 + 3\,\frac{\cos(q\sigma)}{(q\sigma)^2} - 3\,\frac{\sin(q\sigma)}{(q\sigma)^3}\right] \quad (6)$$

with the maximum phonon frequency,

$$\omega_E^2(q) = \left(\frac{4\pi\rho}{3M}\right)\int_0^\infty g(r)V''(r)r^2dr \quad (7)$$

Where M is the atomic mass, ρ the number density and $V''(r)$ the second derivative of the interatomic pair potential, respectively.

While, Takeno and Goda [31, 32] have derived the following expressions for wave vector (q) dependent longitudinal and transverse phonon eigenfrequencies as follows,

$$\omega_L^2(q) = \left(\frac{4\pi\rho}{M}\right)\int_0^\infty dr\; g(r)\left\{\begin{array}{c}\left[r\,V'(r)\left(1-\frac{\sin(qr)}{qr}\right)\right] \\ +\,[r^2V''(r) - rV'(r)] \\ \left(\frac{1}{3} - \frac{\sin(qr)}{qr} - 2\,\frac{\cos(qr)}{(qr)^2} + 2\,\frac{\sin(qr)}{(qr)^3}\right)\end{array}\right\} \quad (8)$$

and,

$$\omega_T^2(q) = \left(\frac{4\pi\rho}{M}\right)\int_0^\infty dr\; g(r)\left\{\begin{array}{c}\left[r\,V'(r)\left(1-\frac{\sin(qr)}{qr}\right)\right]+\\ [r^2V''(r)-rV'(r)]\left(\frac{1}{3}+2\frac{\cos(qr)}{(qr)^2}+2\frac{\sin(qr)}{(qr)^3}\right)\end{array}\right\} \quad (9)$$

According to improved BS model, the phonon frequencies of two branches are represented by [28, 29]

$$\omega_L^2(q) = \frac{2N_C}{\rho q^2}(\beta I_0 + \delta I_2) + \frac{k_e k_{TF}^2 q^2 |G(qr_S)|^2}{q^2 + k_{TF}^2 \varepsilon(q)} \quad (10)$$

and,

$$\omega_T^2(q) = \frac{2N_C}{\rho q^2}\left(\beta I_0 + \frac{1}{2}\delta(I_0 - I_2)\right) \quad (11)$$

with,

$$\beta = \frac{\rho a^2}{2M}\left[\frac{1}{r}\frac{dV(r)}{dr}\right]_{r=a} \quad (12)$$

$$\delta = \frac{\rho a^3}{2M}\left[\frac{d}{dr}\left(\frac{1}{r}\frac{dV(r)}{dr}\right)\right]_{r=a} \quad (13)$$

The notations of $I_0$and I_2 are, with $x = qa$,

$$I_0 = 1 - \frac{sin(x)}{x} \quad (14)$$

and,

$$I_2 = \frac{1}{3} - sin(x)\left[\frac{1}{x} - \frac{2}{x^3}\right] - \frac{2\,cos(x)}{x^2} \quad (15)$$

Here, M, ρ and N_C are the atomic mass, the number density and the coordination number of the said BMGs while $V'(r)$ and $V''(r)$ be the first and second derivatives of the interatomic pair potential, respectively.

For the long-wavelength limit of the phonon frequency spectrum, the longitudinal and transverse frequencies are proportional to the wave vectors as follows [1-14, 18, 19, 23, 24, 28-32] .

$$\omega_L = v_L\, q \quad \text{and} \quad \omega_T = v_T\, q \quad (16)$$

For HB [30], TG [31, 32] and BS [28] approaches respectively, the formulations of longitudinal sound velocity(v_L), and transverse sound velocity(v_T) are given by the following equations,

$$v_L\,(HB) = \omega_E\left(\frac{3}{10}\sigma^2\right)^{1/2} = (0.5477)\omega_E\,\sigma \quad (17)$$

$$v_T\,(HB) = \omega_E\left(\frac{1}{10}\sigma^2\right)^{1/2} = (0.3162)\omega_E\,\sigma \quad (18)$$

$$v_L\,(TG) = \left\{\left(\frac{4\pi\rho}{30M}\right)\int_0^\infty dr\; g(r)\,r^3\,[r\,V''(r) - 4V'(r)]\right\}^{\frac{1}{2}} \quad (19)$$

$$v_T(TG) = \left\{\left(\frac{4\pi\rho}{30M}\right)\int_0^\infty dr\; g(r)\,r^3\,[3r\,V'(r) - 4V'(r)]\right\}^{\frac{1}{2}} \quad (20)$$

$$v_L\,(BS) = \left\{\left(\frac{N_c}{\rho_a}\right)\left[\frac{\beta}{3}+\frac{\delta}{5}\right]+\frac{k_e}{3}\right\}^{\frac{1}{2}} \quad (21)$$

$$v_T(BS) = \left\{\left(\frac{N_c}{\rho_a}\right)\left[\frac{\beta}{3}+\frac{\delta}{15}\right]\right\}^{\frac{1}{2}} \quad (22)$$

For the selected BMGs, some of the important properties viz. isothermal bulk modulus (B_T), rigidity modulus (G), Poisson's ratio (σ), Young's modulus (Y) and Debye temperature θ_D are computed using the expressions as given below [1-14, 18, 19, 23, 24, 28-32].

Isothermal bulk modulus

$$B_T = \rho_M\left(v_L^2 - \frac{4}{3}v_T^2\right) \quad (23)$$

Modulus of rigidity

$$G = \rho_M v_T^2 \quad (24)$$

Poisson's ratio $\sigma = \frac{1}{2}\left[\frac{1-2\left(v_T^2/v_L^2\right)}{1-\left(v_T^2/v_L^2\right)}\right]$ (25)

Young's modulus

$$Y = 2G(\sigma + 1) \quad (26)$$

Debye temperature $\theta_D = \frac{\hbar\,\omega_D}{k_B} =$

$$\frac{\hbar}{K_B}\;2\pi\left(\frac{9\rho}{4\pi}\right)^{\frac{1}{3}}\left(\frac{1}{v_L^3}+\frac{2}{v_T^3}\right)^{-\frac{1}{3}} \quad (27)$$

The input parameters used for present computational work are tabulated in Table 1, which are calculated from using PAA model [1-11] by adopting pure standard data of constituent element of BMGs [41].

Table 1: Input parameters and constants used in present work.

BMG	Z	Z_S	Z_d	R_d(au)	R_s(au)	Ω_0(au)^3	N_C	M (amu)	r_c (au)
$Zr_{67}Ni_{33}$	3.00	1.50	5.20	1.21	1.96	95.02	6.40	46.84	0.6941
$Fe_{80}B_{20}$	3.34	1.50	4.48	2.23	2.10	129.48	12.00	80.49	0.7163

3. Results and Discussion

The discussion and comparison of our present results with available outcomes either theoretical or experimental in the literature are narrated in this section briefly.

3.1 Interatomic pair potential

The pair potentials $V(r)$ (in Ryd.) versus interatomic distance r(au) are displayed in Figs. 1(a) and 1(b) of both BMGs and compared with available theoretical data [12-14]. Also, some theoretical observations from interatomic pair potential curves are presented in Tables 2-3. Though the shape and nature of the interatomic pair potentials appear similar type while the potential well depths related to different BMGs are appeared differently. It is observed that the location of the well-depth of computed pair potentials $V(r)$ moves towards the left for both BMGs as compared to that of reported theoretical data [12-14], which show higher results than the computed one.

The first minima position is significantly affected by the types of screening i.e. the similarity is seen in the pair potential nature by changing the local field correction functions except at or near the dip position. Under the exchange and correlation effect, inclusion in the static H-dielectric screening changes the width and depth of the interatomic pair potential curves. The well-depth impact due to H-correction function is slightly less than that due to the rest of the screening functions. The first zero in the pair potential arises at $r = r_0 = 1.94$ au and 3.76 au for the $Fe_{80}B_{20}$ and $Zr_{67}Ni_{33}$ BMGs respectively. Thus, the effect of exchange and correlation function is not found significantly, but the potential well is more in case of other correlation functions than that of the H-function. Various screening functions influence to increase the well-depth slightly. The maximum and minimum well-depth for $Fe_{80}B_{20}$ is seen due to S- and T-functions, respectively, while the same for the rest of three are lying between them. Similarly, in the case of $Zr_{67}Ni_{33}$, the maximum and minimum well-depths are found for IU- and H-screening functions and the rest of three are lying between them. The interatomic pair potential well-depth deepens with increasing atomic volume and hence here, well-depth of $Fe_{80}B_{20}$ is more than that of $Zr_{67}Ni_{33}$. The potential energy remains negative within the large r-region. The flat type negligible and gradually vanishing oscillations after r =7.31 au and $r =$ 9.61 au in $Fe_{80}B_{20}$ and $Zr_{67}Ni_{33}$ BMGs are observed due to the interaction between electrons and ions because of Colombian repulsion of the potential. However, we have not shown these features correctly from the graph. For the small values of interatomic distances r, the interatomic pair potentials $V(r)$ are strongly repulsive and with the increase of distances, less oscillating nature are observed as expected, which is directly related to the Friedel oscillations due to log-singularity in electron susceptibility function. Moreover, the interatomic pair potentials after the first minima or dip, show minor oscillations of very small amplitude and converges to zero at some larger interatomic distances. In the attractive part, the interatomic pair potentials converge to a limited and fixed value rather than being zero. While, Bretonnet and Derouiche [44] showed that the repulsive part of $V(r)$ is drawn lower and its appealing part is deeper because of the d-electron impact where the $V(r)$ is moved towards the lower r-values and supports the d-electron effect. All pair-potential graphs show the combined effect of s-and d-electrons.

Table 2 : Observations of Interatomic Pair Potentials for $Fe_{80}B_{20}$ BMG.

Screening Function	H	T	IU	F	S
First Zero r (au)	1.94	1.94	1.94	1.94	1.94
Maximum Depth r (au)	2.27	2.25	2.23	2.25	2.25
Maximum Dip (Ryd.)	−0.56	−0.56	−0.57	−0.57	−0.62
Oscillatory Behaviour starts from r (au)	7.92	6.18	6.34	6.07	6.75

Table 3 : Observations of Interatomic Pair Potentials for $Zr_{67}Ni_{33}$ BMG.

Screening Function	H	T	IU	F	S
First Zero r (au)	3.76	3.76	3.76	3.76	3.76
Maximum Depth r (au)	4.44	4.46	4.52	4.51	4.41
Maximum Dip (Ryd.)	−0.10	−0.10	−0.12	−0.11	−0.11
Oscillatory Behaviour starts from r (au)	10.50	12.54	10.43	9.43	10.10

3.2 Phonon dispersion curves

Figures 2-4 show the PDCs of the both BMGs under investigation generated from the interatomic pair potential and pair correlation functions using HB [30]-, TG[31,32]- and BS [28]- approaches with the five screening functions viz. H, T, IU, F and S, respectively. In these PDCs, the longitudinal and transverse modes of phonon eigenfrequencies have been plotted in the form of ω_L and ω_T ($\times 10^{13} s^{-1}$) versus q (Å^{-1}) graphs. Table 4 shows a comparative observational analysis from the PDCs of both BMGs. The presently computed outcomes are compared with available either theoretical [14-16] or experimental data considered by Gupta et al. [13]. The presently obtained results of PDCs are found qualitative agreement with them. Also, the MD result of the Aihara et al. [15,16] of $Zr_{67}Ni_{33}$ BMG at two different temperatures 100K and 500K indicates the low and high amorphous states respectively, which are also shown in the same figure.

For $Fe_{80}B_{20}$ BMG, the first and second ω_L-ω_T crossover positions for the HB [30], TG [31,32] and BS [28] approaches are seen at 2.5 (Å^{-1}) and 3.9; 1.3 (Å^{-1}) and 2.2 (Å^{-1}); 2.3 (Å^{-1}) and 2.6 (Å^{-1}), respectively. For $Zr_{67}Ni_{33}$ BMG, the first and second ω_L- ω_T crossover positions for the HB [30], TG [31,32] and BS [28] approaches are seen at 2.3 (Å^{-1}) and 3.6(Å^{-1}); 1.3(Å^{-1}) and 2.1(Å^{-1}); 2.2(Å^{-1}) and 2.6 (Å^{-1}), respectively. Actually, here model potential parameter r_C is calculated from the well-known formula, which shows significant difference than the reported data. Moreover, the present outcomes of PDCs due to TG [31,32] approach is higher than those due to HB [30] and BS [28] approaches. From the PDCs, the frequency increases with the wave

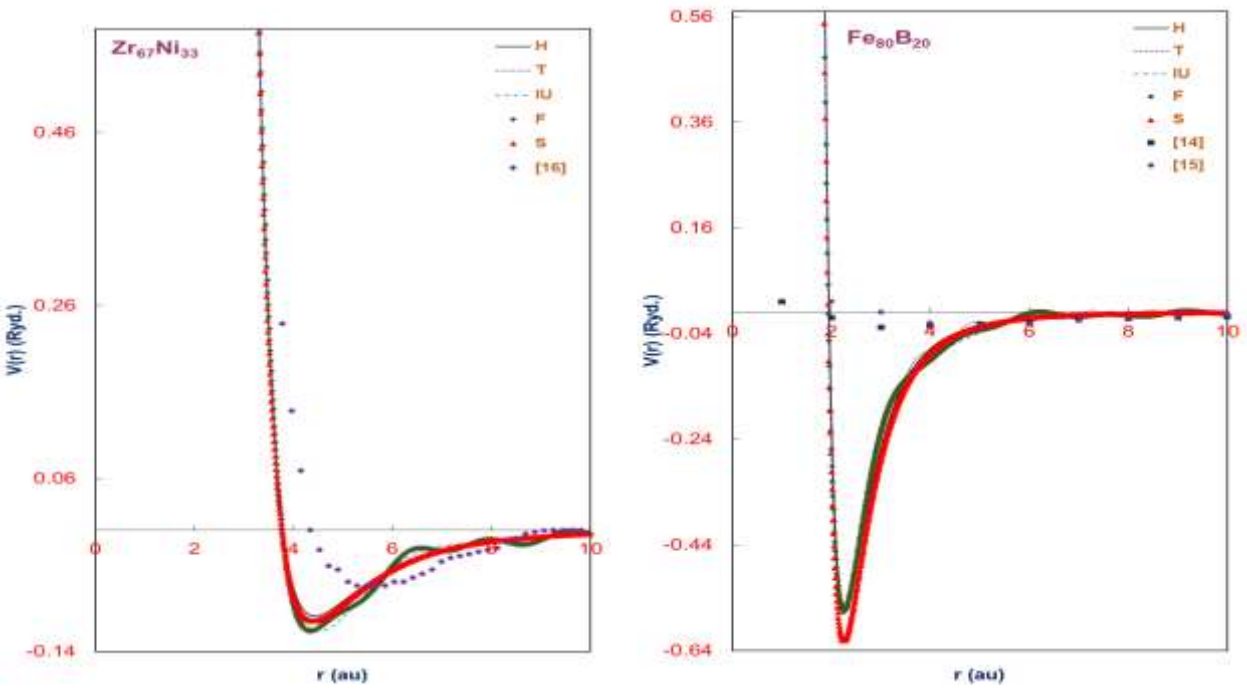

(a) (b)

Fig. 1: Pair potentials for (a) $Fe_{80}B_{20}$ and (b) $Zr_{67}Ni_{33}$ BMGs.

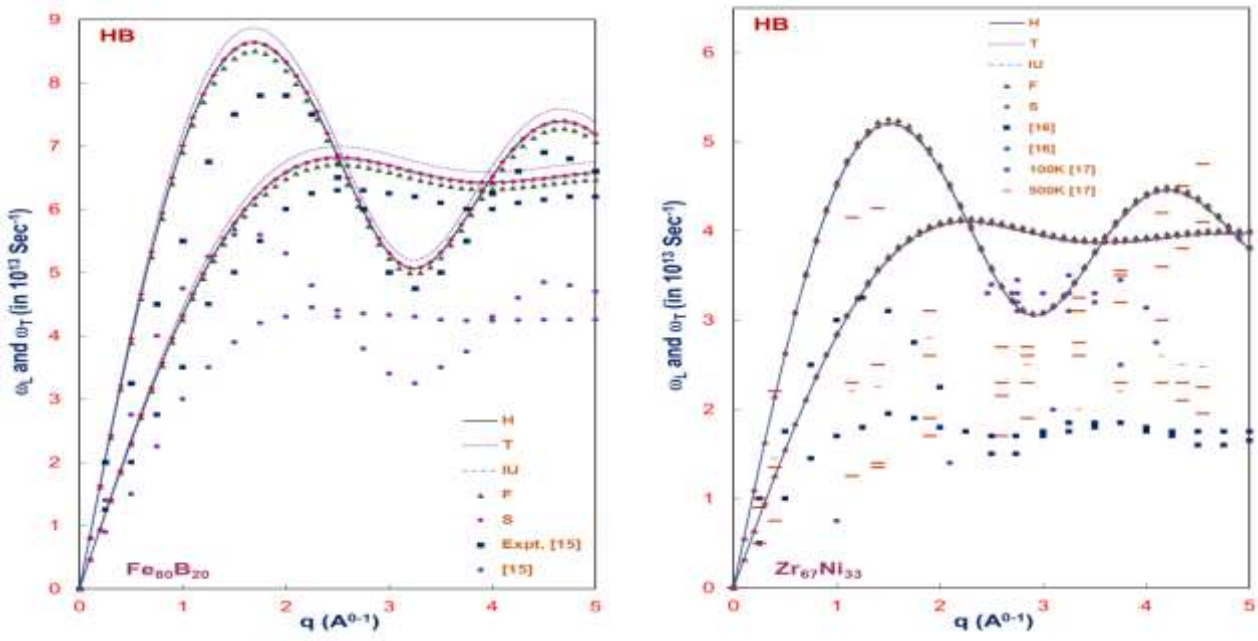

(a) (b)

Fig, 2: Phonon dispersion curves for (a) $Fe_{80}B_{20}$ and (b) $Zr_{67}Ni_{33}$ BMGs using HB approach.

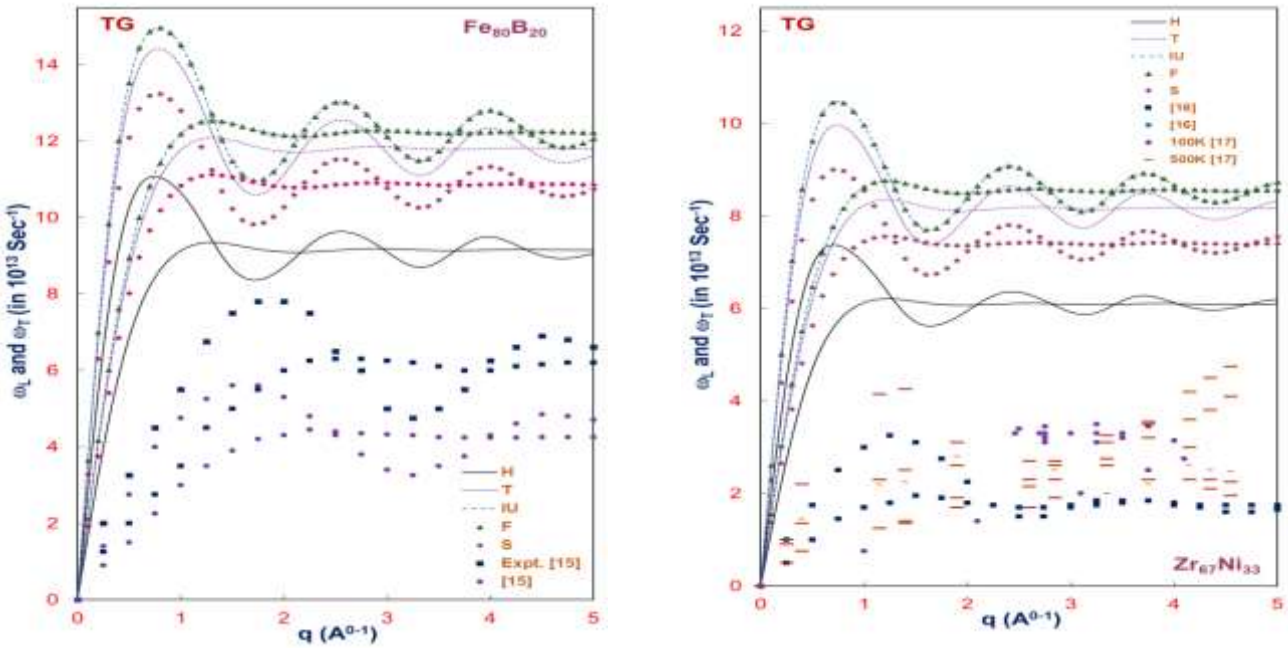

(a) (b)

Fig. 3: Phonon dispersion curves for (a) $Fe_{80}B_{20}$ and (b) $Zr_{67}Ni_{33}$ BMGs using TG approach.

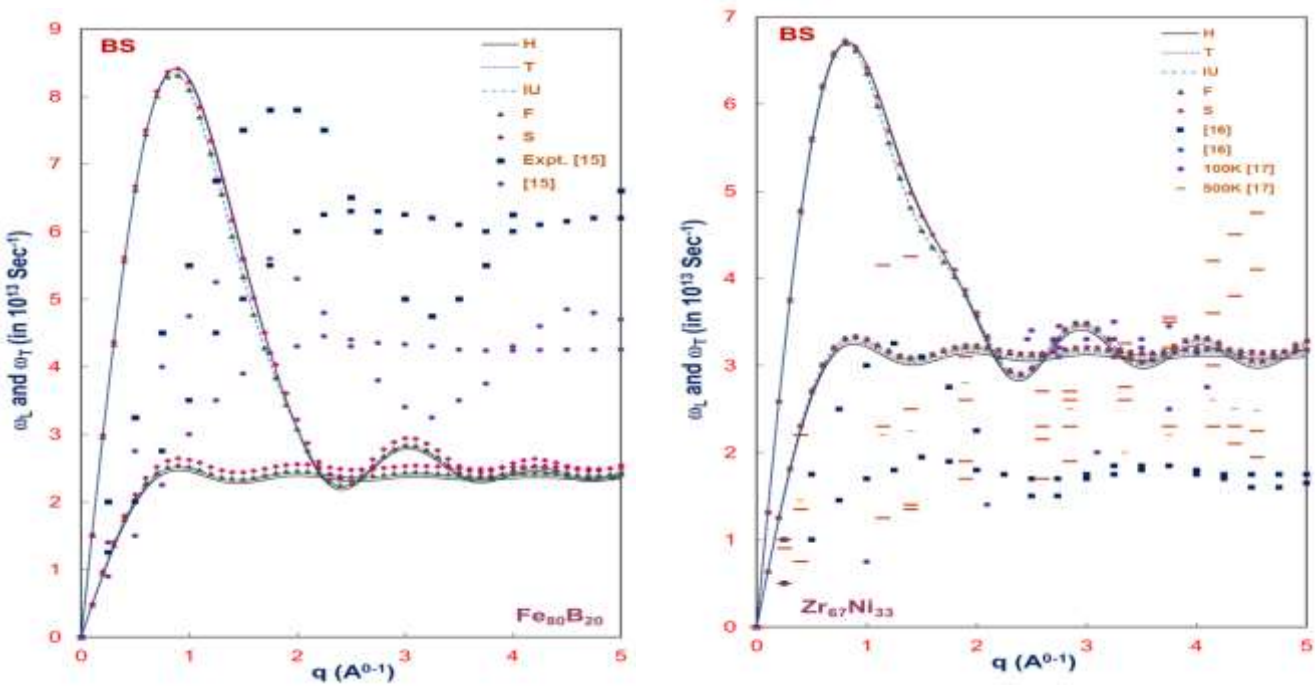

(a) (b)

Fig. 4: Phonon dispersion curves for (a) $Fe_{80}B_{20}$ and (b) $Zr_{67}Ni_{33}$ BMGs using BS approach.

Table 4 : Comparison of the PDCs for the selected binary BMGs.

BMG	Freq.	Order	Maxima $q(\text{Å}^{-1})$			Minima $q(\text{Å}^{-1})$		
			[30]	[31,32]	[28]	[30]	[31,32]	[28]
$Fe_{80}B_{20}$	ω_L	First	1.7	0.7	0.9	3.2	1.7	2.4
		Second	4.7	2.5	3.0	---	3.3	3.7
		Third	---	4.0	4.2	---	4.7	4.7
	ω_T	First	2.5	1.3	0.9	4	2.1	2.6
		Second	---	2.9	3.1	---	3.6	3.7
		Third	---	4.3	4.2	---	---	4.7
$Zr_{67}Ni_{33}$	ω_L	First	1.5	0.7	0.8	2.9	1.6	2.4
		Second	4.2	2.4	2.9	4.8	3.1	3.5
		Third	---	3.7	4.0	---	4.4	4.6
	ω_T	First	2.3	1.2	0.9	3.6	2.0	2.5
		Second	4.8	2.6	3.0	---	3.2	3.5
		Third	---	3.9	4.1	---	4.5	4.6

vector and then saturates after a certain level suggesting that the selected BMGs contain finite liquid clusters, which confirms the Thorpe theory [45]. The transverse phonons are absorbed for such frequencies as they are larger than the smallest eigenfrequencies of the largest cluster.

These PDCs reveal that the oscillations are more prominent in longitudinal phonon modes than those in the transverse phonon modes in the large wave vector transfer region, which corresponds to the fluctuations in the particle density of these BMGs and therefore, approves the presence of the short-wavelength collective excitations. The instability in the transverse mode oscillations is due to the anharmonicity of the atomic vibrations, which suggests the transverse phonons undergo a large thermal modulation. The fluctuations in the transverse phonon mode decrease out rapidly, which connects to the damping transverse phonon modes in BMGs. In the lower wave vector transfer region, the PDCs are linear due to the characteristics of the elastic waves; but for the higher wave vector region, this linear relationship does not hold, as the sound velocity is different for different wave vectors. The collective excitations at larger wave vector transfer are due to the eminence of the longitudinal mode excitations only. The longitudinal part of PDC shows that the BMGs are screening sensitive in the low momentum region. The difference in the ω_L or ω_T (s^{-1}) versus q (Å^{-1}) exists from the beginning, becomes maximum at the peak point and again decreases till the dip point. The peak height is dependent on the screening function as well as on the applied pseudopotential approach. The longitudinal PDCs display oscillatory behavior for larger q values, which is absent in case of transverse phonons. A longitudinal phonon curve reaches maxima at a higher q value than the transverse one. Comparatively, the longitudinal frequency bears higher numerical value than the transverse frequency for a particular q value, which is reflected by the distance between their peak or deep positions. For all three approaches, the transverse phonon frequencies grow with wave number and

become saturated at the first peak with small variations. Though the first peak position is independent of the screening functions, the peak-height is fairly dependent on the screening function used in this computational work. From the second and third ordered minima and maxima for any screening functions in the HB [30]-approach do not appear clearly. The selected BMGs are screening sensitive in the low-momentum region. Furthermore, the phonons are detected as sound waves in the macroscopic frequency limits of the spectrum. Hence, the longitudinal sound velocity (v_L) and transverse sound velocity (v_T) have been estimated from the linear part of their curves.

3.3 Computed properties

The computed elastic and thermodynamic properties of $Fe_{80}B_{20}$ and $Zr_{67}Ni_{33}$ BMGs with the available reference data are presented by Tables 5 and 6 respectively, from which, it appears that the calculated values of different properties nearly agree to each other for different screening functions for a particular approach but considerably differs for different approaches i.e. a property holds nearly the same value for all screening functions for a particular approach, but the same property holds different values for the same screening function in another approach. For the selected binary glasses, our presently computed outcomes from HB and BS approaches are found in fair qualitative agreement with available results [2, 5, 13-16, 19, 21]. Our results are over estimated with them.

It is quite tough to judge that which of the three approaches adopted here is the best suitable for computation of vibrational dynamics of aforesaid binary BMGs, because each approach has its own identity, importance and limitations too. The HB approach is an older one but simple enough to need a minimum number of parameters to produce consistent results of the phonon data. While, the TG [31,32] approach is established upon the quasi-crystalline approximation, where effective force constant depends upon the correlation function for the displacement of atoms, which further depends on the phonon frequencies. Similarly, the BS approach retains interatomic interactions effectively between the first nearest neighbours only. Therefore, the atomic disorderedness in the formation of metallic glasses is more which show a deviation in the magnitude of PDCs and their concerned properties.

The dielectric function plays an significant role in the estimation of potential due to the screening of the electron gas. For this determination, in the present study, the local filed correction function due to H, T, IU, F and S are taken. Motive for choosing them is that, the H-function does not include exchange and correlation effect and signifies only static dielectric function, whereas the T-function cover the overall features of the numerous local field correction functions projected before 1972. The IU, F and S functions are newer one amongst the existing functions and not exploited thoroughly in current study. This helps us to study the comparative effects of exchange and correlation in the aforementioned properties. Therefore, the present outcomes found from five dissimilar local field correction functions may be as in contract with each other, as different order of magnitude in the Figures 1-4.

Table 5: Thermodynamic and elastic properties of $Fe_{80}B_{20}$ BMG.

Approach	Scr. Fun.	$v_L \times 10^5$ (cm/s)	$v_T \times 10^5$ (cm/s)	$B_T \times 10^{11}$ d(yne/s^2)	$G \times 10^{11}$ (dyne/s^2)	σ	$Y \times 10^{11}$ (dyne /s^2)	θ_D K
[30]	H	8.23	4.75	20.78	12.47	0.25	31.17	650.71
	T	8.44	4.87	21.84	13.10	0.25	32.76	667.12
	IU	8.19	4.73	20.60	12.36	0.25	30.90	647.89
	F	8.09	4.67	20.10	12.06	0.25	30.15	639.96
	S	8.23	4.75	20.76	12.46	0.25	31.14	650.37
[31, 32]	H	28.70	16.71	249.04	154.27	0.24	383.59	2287.08
	T	35.81	20.86	387.68	240.19	0.24	597.23	2853.78
	IU	36.94	21.52	412.74	255.72	0.24	635.84	2944.58
	F	36.94	21.52	412.69	255.68	0.24	635.75	2944.39
	S	33.32	19.41	335.73	208.00	0.24	517.19	2655.68
[28]	H	8.14	2.53	31.84	3.53	0.45	10.22	355.28
	T	8.16	2.57	31.92	3.66	0.44	10.57	361.53
	IU	8.16	2.61	31.80	3.76	0.44	10.85	366.48
	F	8.17	2.62	31.83	3.80	0.44	10.97	368.47
	S	8.26	2.70	32.25	4.04	0.44	11.63	379.60
Others-[30] Vora [5]	H	3.86	2.23	5.98	3.59	0.25	8.98	333.79
	T	3.39	1.96	4.61	2.77	0.25	6.92	293.04
	IU	3.67	2.12	5.43	3.26	0.25	8.15	318.01
	F	3.66	2.11	5.39	3.23	0.25	8.09	316.78
	S	1.66	0.96	1.11	0.67	0.25	1.67	143.82
Others-T[31,32] Vora [5]	H	4.85	2.08	12.87	3.14	0.39	8.72	317.80
	T	4.69	2.26	11.04	3.69	0.35	9.96	342.58
	IU	4.91	2.27	12.47	3.75	0.36	10.22	345.93
	F	4.94	2.31	12.55	3.86	3.36	10.50	350.98
	S	3.30	1.89	4.42	2.59	0.25	6.50	283.61
Others-[28] Vora [5]	H	9.49	3.56	53.06	9.16	0.42	25.99	545.01
	T	9.61	3.71	53.64	9.95	0.41	28.11	567.51
	IU	9.58	3.67	53.41	9.74	0.41	27.53	561.47
	F	9.57	3.67	53.38	9.73	0.41	27.53	561.41
	H	9.65	3.74	53.86	10.13	0.41	28.60	572.69
Others [21]		---	---	13.80 17.40	7.60 5.00	---	---	169.00 169.30
Expt. [21]		---	---	14.10	6.50	---	---	---

Table 6 : Thermodynamic and elastic properties of $Zr_{67}Ni_{33}$ BMG.

Approach	Scr. Fun.	$v_L \times 10^5$ (cm/s)	$v_T \times 10^5$ (cm/s)	$B_T \times 10^{11}$ (dyne/s^2)	$G \times 10^{11}$ (dyne/s^2)	σ	$Y \times 10^{11}$ (dyne/s^2)	θ_D K
[30]	H	5.49	3.17	11.67	7.00	0.25	17.51	391.75
	T	5.50	3.18	11.70	7.02	0.25	17.55	392.25
	IU	5.47	3.16	11.59	6.95	0.25	17.38	390.34
	F	5.55	3.20	11.91	7.15	0.25	17.87	395.71
	S	5.49	3.17	11.66	7.00	0.25	17.49	391.51
[31,32]	H	19.61	11.51	144.94	92.21	0.24	228.22	1419.31
	T	25.51	14.99	244.58	156.50	0.24	386.96	1848.80
	IU	26.60	15.63	265.81	170.20	0.24	420.78	1927.97
	F	26.61	15.64	265.92	170.26	0.24	420.95	1928.35
	S	23.36	13.72	205.16	131.07	0.24	324.18	1692.01
[28]	H	7.61	3.65	27.93	9.29	0.35	25.09	456.96
	T	7.65	3.69	28.09	9.50	0.35	25.61	461.92
	IU	7.68	3.74	28.09	9.74	0.34	26.20	467.54
	F	7.70	3.75	28.17	9.82	0.34	26.38	469.27
	S	7.72	3.76	28.40	9.85	0.34	26.48	470.03
Others [14]		4.46	1.88	10.40	2.43	---	---	236.00
Others-MD [15,16]		4.10 4.75	1.95 2.02	7.80 11.72	2.80	---	---	217.00 254±11
Others-[14,30]		5.00	2.50	11.76	---	---	---	311.00
Others-[14, 28]		4.19	2.05	8.46	---	---	---	256.00
Others [19]		3.53	2.04	4.94	2.96	---	7.40	---
Others-[30] Vora [2,3]	H	1.79	1.03	1.25	0.75	0.25	1.87	127.87
	T	1.81	1.04	1.27	0.76	0.25	1.91	129.23
	IU	0.87	0.50	0.29	0.18	0.25	0.44	62.10
	F	0.85	0.49	0.28	0.17	0.25	0.42	60.80
	S	1.59	0.92	0.99	0.59	0.25	1.48	113.73
Others-[31,32] Vora [2,3]	H	2.41	1.37	2.34	1.31	0.26	3.30	169.30
	T	2.80	1.61	3.06	1.83	0.25	4.57	199.80
	IU	2.72	1.70	2.49	2.03	0.17	5.02	214.60
	F	2.78	1.75	2.55	2.14	0.17	5.02	214.60
	S	2.40	1.48	2.01	1.53	0.20	3.66	181.70
Others-[28] Vora [2,3]	H	7.18	3.44	25.02	8.32	0.35	22.46	431.84
	T	7.30	3.57	25.45	8.93	0.34	23.97	446.91
	IU	7.25	3.52	25.28	8.69	0.35	23.38	441.08
	F	7.23	3.50	25.14	8.60	0.35	23.16	438.94
	S	7.36	3.62	25.75	9.21	0.34	24.68	453.72

4. Conclusion

Lastly, the computed PDCs of the BMGs have satisfactorily reproduced the general characteristic features of a broad range of collective excitations. The presently computed PDCs and their concerned properties through HB, TG and BS approaches have shown consistent results with the successful application of the Shaw's model pseudopotential, where screening effects are also observed by various local field correction functions, which supports the PAA model and pseudopotential concept. The screening effect plays a significant role in the estimation of the thermodynamic and elastic properties of said BMGs. The relative exchange and correlation effects in the selected properties are successfully examined by H-, T-, IU-, F- and S- local filed correction functions, which show variations according to the vibrational properties. The calculated properties observed at room temperature are found in qualitative agreement with acceptable differences with the data available in the literature. The PDC generated from the three approaches are satisfactorily reproduced general characteristics of dispersion curves. The thermodynamic and elastic properties obtained due to TG [31, 32]-approach are higher than those due to HB [30] or BS [31, 32]-approaches. Hence, the pseudopotential theory is remarkably helpful for the framework of computation of theoretical data for a specific BMG.

References

[1] A. M. Vora, Vibrational dynamics of non-crystalline glassy alloys, Front Mater Sci China 1(4) (2007) 366-378. https://doi.org/10.1007/s11706-007-0068-z

[2] A. M. Vora, Vibrational dynamics of Ni-glassy alloys, Front Mater Sci China 3 (2009) 285-300. https://doi.org/10.1007/s11706-009-0045-9

[3] A. M. Vora, Vibrational dynamics of bulk metallic glasses studied by pseudopotential theory, In: Oster WU (ed) Computational materials, Nova Science Publishers, Inc., New York, 2009, pp 119-176.

[4] A. M. Vora, Vibrational dynamics of binary metallic glasses, J Non-Oxide Glasses 1(2) (200) 157-173.

[5] A. M. Vora, Vibrational dynamics of Fe-based glassy alloys, Front Chem China 6(2) (2011) 127-141. https://doi.org/10.1007/s11458-011-0236-7

[6] A. M. Vora A. L. Gandhi, Phonon dynamics of bulk metallic glass using takeno-goda approach, Armenian J Phys 12(4) (2009) 289-294.

[7] A. L. Gandhi, A. M. Vora, Theoretical study of Pd39Ni10Cu30P21 bulk metallic glass using TG and BS approaches, KCG e-j Sci 19 (2019) 1-8.

[8] A. L. Gandhi, A. M. Vora, Theoretical study of thermodynamic and elastic properties of Ti50Be34Zr16 BMG – A pseudopotential method, Internat J Trend Sci Res Dev 3(2) (2019) 1076-1080.

[9] A. L. Gandhi, A. M. Vora, A pseudopotential study on the thermodynamic and elastic properties of Pd39Ni10Cu30P21 bulk metallic glass, Research Guru 12(4) (2019) 1-10. https://doi.org/10.31142/ijtsrd21550

[10] A. M. Vora, A. L. Gandhi, Collective dynamics of Zr-based bulk metallic glasses, Chinese J Phys 62 (2019) 284-295. https://doi.org/10.1016/j.cjph.2019.10.013

[11] A. M. Vora, R. C. Malan, Vibrational dynamics of Pd39Ni10Cu30P21 bulk metallic glass, Materials Today: Proc 12(3) (2019) 549–553. https://doi.org/10.1016/j.matpr.2019.03.097

[12] C. H. Hausleitner, I. Turek, Structural, electronic, and magnetic properties of metallic glasses, J Non-Cryst Sol 156 (1993) 210-218. https://doi.org/10.1016/0022-3093(93)90165-T

[13] A. Gupta, D. Bhandari, N. S. Saxena, Vibrational dynamics of amorphous Fe80B20, Ind J Pure & Appl Phys 36 (1998) 366-369.

[14] A. Gupta, A. Prasad, D. Bhandari, K. C. Jain, N. S. Saxena Vibrational dynamics of $Zr_{67}Ni_{33}$ amorphous alloy, J Phys Chem Sol 58 (1997) 33-37. https://doi.org/10.1016/S0022-3697(96)00104-7

[15] Jr. T. Aihara, Y. Kawazoe, T. Masumoto Molecular dynamics simulation for binary amorphous Zr-Ni alloys, J. Non-Cryst Sol 205-207 (1996) 875-878. https://doi.org/10.1016/S0022-3093(96)00474-7

[16] Jr. T. Aihira, T. Masumoto, Dispersion of collective excitations of amorphous and liquid $Zr_{67}Ni_{33}$ alloys, J Phys: Conden Matt 7(1995) 1525-1541. https://doi.org/10.1088/0953-8984/7/8/003

[17] T. Otomo, M. Arai, J. B. Suck, S. M. Bennington M (2002) An experimental approach to reveal the origin of collective excitations in Ni33Zr67 metallic glass, J Non-Cryst Sol 599 (2002) 312-314. https://doi.org/10.1016/S0022-3093(02)01792-1

[18] K. N. Lad, A. Pratap, Phonon dispersion in amorphous Zr-Ni alloys, Physica B 334 (2003) 135-146. https://doi.org/10.1016/S0921-4526(03)00039-5

[19] D. Singh, Y. Sonavane, P. Thakore, Vibrational properties of Zr-Ni Metallic Glasses, Materials Today: Proc 3 (2016) 3137-3143. https://doi.org/10.1016/j.matpr.2016.09.030

[20] K. Sugita, M. Mizuno, H. Araki, Y. Shirai, Electronic structure and bonding in amorphous $Zr_{67}Ni_{33}$ and $Zr_{67}Cu_{33}$, Adv Quantum Chem 54 (2008) 161-173. https://doi.org/10.1016/S0065-3276(07)00013-5

[21] C. Suryanarayana, A. Inou, Iron-based metallic glasses, International Material Reviews 58(3) (2013)131-166. https://doi.org/10.1179/1743280412Y.0000000007

[22] V. I. Dimitrov, Y. I. Klechin, A. V. Apostolov, Calculation for elastic moduli for Fe80B20, Phys Stat Sol (a) 116 (1989) 627-632. https://doi.org/10.1002/pssa.2211160221

[23] P. C. Agarwal, C. M. Kachhava, Phonon dispersion in metallic glass Mg70Zn30, Physica B 179(1) (1992) 43-47. https://doi.org/10.1016/0921-4526(92)90618-3

[24] P. C. Agarwal, C. M. Kachhava, Phonon Frequencies in Metallic Glasses, Phys Stat Sol (b) 179 (1993) 365-371. https://doi.org/10.1002/pssb.2221790211

[25] P. Lamparter, S. Steeb, In: Cahn RW,Haasen P, Kramer EJ (eds) Materials Science, and Technology-Vol.1, VCH, Weinheim, 1993, pp.217

[26] E. Nassif, P. Lamparter, W. Sperl , S. Steeb, Structural investigation of the metallic glasses Mg85.5Cu14.5 and Mg7oZn3o, Z. Naturforsch 38a (1983) 142-148. https://doi.org/10.1515/zna-1983-0208

[27] E. Nassif, P. Lamparter, W. Sperl , S. Steeb) X-Ray diffraction study on the structure of the metallic glasses Mg84Ni16 and Mg30Ca70, Z. Naturforsch 38a (1983) 1206-1209. https://doi.org/10.1515/zna-1983-1106

[28] A. B. Bhatia, R. N. Singh, Phonon dispersion in metallic glasses: A simple model, Phys Rev B 31(8) (1985) 4751-4758. https://doi.org/10.1103/PhysRevB.31.4751

[29] M. M. Shukla, J. R. Campanha , Lattice dynamics of metallic glass Ca70Mg30 on the model of Bhatia and Singh. Acta Phys Polo A 94(4) (1998) 655-660. https://doi.org/10.12693/APhysPolA.94.655

[30] J. Hubbard, J. L. Beeby, Collective motion in liquids, J Phys C: Solid State Phys 2(3) (1969) 556-571. https://doi.org/10.1088/0022-3719/2/3/318

[31] S. Takeno, M. Goda, A theory of phonons in amorphous solids and its implications to collective motion in simple liquids, Prog Theor Phys 45(2) (1971) 331-352. https://doi.org/10.1143/PTP.45.331

[32] S. Takeno, M. Goda, A theory of phonon like excitations in non-crystalline solids and liquids, Prog Theor Phys 47(3) (1972) 790-806. https://doi.org/10.1143/PTP.47.790

[33] J. B. Suck, H. Rudin, H. J. Guntherodt, H. Back, In: Steeb S, Warlimont H (eds) Proceedings of the 5th international conference on rapidly quenched metals, North- Holland, Amsterdam, 1985 pp 471. https://doi.org/10.1016/B978-0-444-86939-5.50114-7

[34] N. W. Ashcroft, Electron-ion pseudopotentials in metals, Physics Lett. 23 (1966) 48-50. https://doi.org/10.1016/0031-9163(66)90251-4

[35] L. A. Davis, R. Ray, C. -P. Chou, R. C. O' Handley, Mechanical and thermal properties of Fe80B20 glass, Scripta Met 10 (1976) 541-545. https://doi.org/10.1016/0036-9748(76)90257-X

[36] R. W. Shaw, Optimum form of a modified Heine-Abarenkov model potential for the theory of simple metals, Phys Rev 174(3) (1968) 769-781. https://doi.org/10.1103/PhysRev.174.769

[37] W. A. Harriso, Elementary Electronic Structure, World Scientific, Singapore, 1999.

[38] R. Taylor, A simple, useful analytical form of the static electron gas dielectric function, J Phys F: Metal Phys 8 (1978) 1699-1702. https://doi.org/10.1088/0305-4608/8/8/011

[39] S. Ichimaru, K. Utsumi, Analytic expression for the dielectric screening function of strongly coupled electron liquids at metallic and lower densities, Phys Rev B. 24(12) (1981) 7385-7388. https://doi.org/10.1103/PhysRevB.24.7385

[40] A. Sarkar, D. S. Sen, S. Haldar, D. Roy, Static Local Field Factor for Dielectric Screening Function of Electron Gas at Metallic and Lower Densities, Modern Phys Lett B. 12(6) (1998) 639-648. https://doi.org/10.1142/S0217984998000755

[41] J. M. Wills, W. A. Harrison, Interionic interactions in transition metals, Phys Rev B28 (1983) 4363-4373. https://doi.org/10.1103/PhysRevB.28.4363

[42] P. Lamparter, S. Steeb, E. Grallath, Neutron diffraction study on the structure of the metallic glass Cu57Zr43, Z Naturforsch 38a(1983)1210-1222. https://doi.org/10.1515/zna-1983-1107

[43] E. T. Faber, Introduction to the Theory of Liquid Metals, Cambridge Uni. Press, London, 1972.

[44] J. L. Bretonnet, A. Derouiche, Variational thermodynamic calculations for liquid transition metals, Phys Rev B 43 (1990) 8924-8929. https://doi.org/10.1103/PhysRevB.43.8924

[45] M. F. Thorpe, Continuous deformation in random networks, J Non-Cryst Sol 57(3) (1983) 355-370. https://doi.org/10.1016/0022-3093(83)90424-6